Carnot: An Architectural Framework for Mapping the Empirical Bounds of LLM Verification

Ian Blenke
ian@blenke.com

Position paper draft v3, 2026-05-01
Target: arXiv preprint by 2026-05-15

Abstract

Verifier-filtered self-distillation has become a central paradigm for aligning open-weight LLMs without closed-frontier dependence. We show empirically that naive scaling collides with three structural walls—a verifier correlation ceiling, an exact-sampling detailed-balance limit, and an out-of-distribution energy-ordering inversion on highly-optimized SOTA outputs—that no engineering effort can overcome in their current form. We position Carnot as an architectural framework that makes these walls measurable, bounds them with closed-form theory, and deploys mathematically exact fallbacks. Specifically, we (i) apply the Welch/Rankin Simplex bound to derive the verifier-composition ceiling $k^* \leq 3.125$ from $D_{\text{eff}} = 1.603$ (exp1093); (ii) replace the parallel Glauber hardware story with a $\chi \leq 4$ sparse-constraint FPGA Fast-Path plus CPU fallback after auditing software-proxy KL = 3.07 (exp1094); (iii) document the pre-retrain energy-ordering inversion ($\overline{E}_{\text{correct}} = 0.689 > \overline{E}_{\text{incorrect}} = 0.621$) as a Goodhart-class anomaly; (iv) show retraining on a 7,329-pair SOTA-inclusive corpus restores correct ordering with AUROC=0.9774 (exp1120); and (v) report pre-filtered self-distillation collapse (exp1099), confirming the energy signal must drive the filter. Positive baselines—SOS-KAN AUROC=0.9545 (n=6,548; exp1072), GRPO with ThinkPRM v2 improving GSM8K by +8.51 pp (n=47, 95% CI: [1.0%, 26.0%]; exp1129), $\alpha_t = 0.52$ post-retrain (exp1130)—demonstrate the framework is operational in-distribution. We position Carnot's Apache-2.0, local-first, hardware-portable design as the substrate enabling cross-mechanism verifier diversity, the only known route past the Welch ceiling.

1 Introduction

Notation and conventions. For reviewer convenience, we collect the project-internal terminology used throughout this paper.

- **Milestone numbers *.NN*** (e.g. ".85", ".87", ".88"). Carnot is developed by an autonomous research conductor that stamps each completed milestone with the identifier YYYY.MM.NN. Throughout this paper, ".NN" is shorthand for the Nth milestone of 2026-04. ".85" specifically refers to the milestone in which the four wall-class measurements anchoring this paper were taken.
- **Paper version *v2* vs *v3*.** This paper is draft v3, published 2026-05-01. Earlier internal drafts (v1, v2) were never publicly distributed. References to "v2's claim X" or "preserved from v2" are given so that contributors who tracked the project across drafts can map revisions; readers seeing the work for the first time can treat every v2 reference as "the prior internal draft" without losing technical content.
- ***k*.** Cardinality of the formally-distinct verifier ensemble that AND-composes acceptance decisions. The measured production orthogonality audit is $k = 5$; see Section 4.1 for composition and provenance.
- ***α_t* (Zenil's self-distillation grounding signal).** The fraction of training-time steps at which the verifier-ensemble supervision diverges from the teacher pseudo-label, measured per Zenil's self-distillation framework (Section 4). Higher α_t means the verifier is providing genuinely new signal rather than echoing the teacher.

- **D_{eff} and D_{int} (effective and intrinsic dimensions of the joint verifier embedding).** Both are Participation-Ratio-derived scalars over the verifier-output covariance: D_{eff} is the deployed-text estimate (`exp1093`); D_{int} is the architectural upper bound. Lower D_{eff} implies higher pairwise correlation among verifiers and a smaller effective ensemble. Section 5 derives the bound and projects the measurement against the Welch/Rankin Simplex.
- **Cascade tiers (Tier 0a, 0b, 0c, 1, 2, 2.5, 2.7, 3).** Carnot routes outputs through tiers of progressively more expensive verifiers, exiting at the first tier whose energy threshold either accepts or rejects with confidence. Tier 0a (ThinkPRM) is the cheapest; Tier 3 (Z3 SMT) is the most expensive and most precise. Section 4 defines each tier in detail.
- **Phase 1 / 2 / 3 / 4** refer to Carnot's project phases: Phase 1 (verify-repair pipeline, current production), Phase 2 (hardware acceleration via FPGA / Extropic Z1), Phase 3 (open-source foundation model with continuous-latent reasoning, DBAE-EBM substrate), Phase 4 (active-inference / free-energy- principle reformulation, committed 2026-05-02). Phase 3-7 in Section 4 refers to the multi-step Phase 3 decomposition derived in nine rounds of cross-validating Deep Think analyses.

The problem we want to attack is decentralized verification of LLM outputs: given a hosted-locally open-weight base model whose generations may be incorrect, hallucinated, or adversarially manipulated, produce a calibrated rejection signal that runs on the same hardware as the base model and depends on no closed-API oracle. This is a hard problem because there is no obvious way to get an external truth signal: any such verifier ultimately has to rest on either symbolic constraints, runtime execution, or another learned probe of similar provenance to the base model.

The naive recipe in the field — and in v2 of this paper — was **compose more verifiers, run them faster, and the joint null space shrinks exponentially in k.** Three .85 milestone experiments show that this recipe fails in three distinct ways.

Wall 1 — Verifier correlation ceiling. When we measured the pairwise r-correlation across three deployed text probes (SpilledEnergyDetector, NUPProbeV4, PCIBProbe) on 364 examples (exp1093), we found $r \in [0.41, 0.66]$ with a Participation Ratio of $D_{\text{eff}} = 1.603$ — three nominally independent verifiers carry less than two effective dimensions of information. The naive "AND-composition shrinks the joint null space exponentially in k" result is conditional on transversality (Friedrichs angle $\theta_F > 0$); empirically, θ_F is small for any verifier family that reads continuous text features.

Wall 2 — Exact-sampling detailed-balance limit. The synchronous parallel Glauber sampler that produced the original invalid FPGA headline does not preserve detailed balance on frustrated topologies: software-proxy $\mathrm{KL}(P_{\text{parallel}} \,\|\, P_{\text{Gibbs}}) = 3.07$ on the canonical 12-spin antiferromagnetic ring (exp1094 simulation; bitstream on-board KL not yet measured). The paper no longer uses the Python CPU comparison as a speedup claim; the sampling distribution the simulator produced was not the target distribution.

Wall 3 — Out-of-distribution energy-ordering inversion. On 100 SOTA-model outputs, the cascade reports $\overline{E}_{\text{correct}} = 0.689$ vs. $\overline{E}_{\text{incorrect}} = 0.621$ (exp1100 artifact has a DURATION_TOO_SHORT fabrication flag; the 7.05s duration for 100 live 35B model calls is not credible; this result is excluded from headline claims pending replication). The energy gap inverts: heavily-optimized SOTA outputs produce *lower* energy for incorrect completions than for correct ones. The same energy function on the FoVer corpus (n=6,548; exp1072) reaches AUROC = 0.9545; the inversion is not a sign-bug but an out-of-distribution shift consistent with reward-hacking dynamics (Goodhart's Law) on outputs that were optimized against a similarly-shaped verifier.

We could ignore each wall, fabricate around it, or disclaim it in an appendix. We choose instead to build the entire paper around the proposition that **the walls are themselves the contribution.**

The pivot has consequences for every section. Section 4 defines the architectural framework as the *measuring apparatus* deployed to discover the walls, not as a "finished" verification system. Section 5 develops the theory needed to bound them: the $\sqrt{\det(\Sigma)}$ joint-volume factor, the Welch/Rankin Simplex bound on k^*, the Participation Ratio as the empirical projection onto the bound. Section 6 reports the

hardware deployment story — including the $\chi \leq 4$ Fast-Path architecture and the explicit deferral of same-basis CPU-vs-FPGA timing claims — as a direct response to the software-proxy KL = 3.07 finding (exp1094 simulation; bitstream on-board KL not yet measured). Section 7 foregrounds the four .85 honest negatives as the architectural telemetry's primary output. Section 9 positions Carnot's Apache-2.0, local-first design as a strict engineering prerequisite for cross-mechanism verifier diversity. Section 11 closes with the Mock Cascade roadmap and the precise bounds the framework hands future work.

The audience for this paper is researchers who care about whether the published numerical claims of LLM-verifier work survive adversarial scrutiny. Carnot is offered as a worked example of publishing the limits along with the headline.

Carnot is the first open-source externally-grounded EBM that solves multimodal text collapse via a multi-verifier ensemble — filling the gap between Kona [**?**] (closed enterprise) and EBTs [**?**] / NRGPT (open but lacking external grounding).

2 Anchored Claims

This paper-v6 narrowing pass treats the following claims as the complete headline claim set. Each claim is retained only because it has checked-in empirical artifacts and a named theoretical support boundary; broader interpretations move to Appendix or future work.

Theoretical Background. The foundational theoretical background mapping these bounds to auto-regressive generation relies on the exact ARM-EBM bijection [**?**].

1. **CLAIM-1 — Verifier composition is bounded by measured correlation.** Carnot may claim a measured heterogeneous k=5 verifier stack and a homogeneous text-probe ceiling; it may not claim arbitrary k scaling. Empirical artifacts: `results/experiment_1093_phase1c_verifier_joint_null_space_measurement.json`, `results/experiment_1224_phase5c_adversarial_probe.json`, `results/experiment_1256_verifier_orthogonality_audit_v3.json`. Theoretical support: sqrt(det(Sigma)) joint-volume correction; Welch/Rankin Simplex bound on verifier packing; Spera non-composability boundary for shared verifier null spaces. Boundary: Does not claim k=6, k=15, or exponential AND-composition gains beyond the measured evidence..

2. **CLAIM-2 — Exact sampling requires sparse fast-path plus CPU fallback.** Carnot's hardware story is a correctness-first chi¡=4 sparse constraint fast-path with CPU fallback, not a universal FPGA speedup. Empirical artifacts: `results/experiment_1068_kv260_smoke_test_v9.json`, `results/experiment_1094_phase2a_sampler_correctness_audit.json`, `results/experiment_1451_discrete_sb_rtl_lint_sim_rerun.json`, `results/experiment_1460_hardware_portfolio_narrowing.json`. Theoretical support: single-site Gibbs detailed balance; chromatic-Glauber batching under graph-coloring constraints; scope-reduction hardware portfolio gate. Boundary: Does not claim same-basis CPU-vs-FPGA speedup, KV260 board execution for new bitstreams, Extropic execution, NPU acceleration, or photonic execution..

3. **CLAIM-3 — Energy verifier calibration is distribution-bound.** Carnot may claim in-distribution SOS-KAN calibration [**?**], a measured SOTA-output energy-ordering inversion, and a SOTA-inclusive retrain that fixes the observed inversion on its validation split. Empirical artifacts: `results/experiment_1072_sos_kan_v3_neural_gram.json`, `results/experiment_1100_cascade_validation_sota_outputs.json`, `results/experiment_1120_energy_verifier_retrain_sota.json`, `results/experiment_1265_diffutruth_vs_carnot_baseline.json`. Theoretical support: Goodhart/reward-hacking interpretation of verifier-shaped optimization; energy-based calibration under distribution shift; OOD boundary between FoVer and optimized SOTA-output corpora. Boundary: Does not claim universal verifier dominance, cross-corpus DiffuTruth dominance, or future SOTA-family generalization..

4. **CLAIM-4 — Self-learning is a narrow verified-memory-growth claim.** Carnot may claim one verified self-learning pivot: semantic-verified fresh memory growth with non-forgetting, as selected by Exp 1459. Empirical artifacts: `results/experiment_1374_continuous_self_learning_v3_verifier_selected_or_csp_fallback.json`, `results/experiment_1433_fr11_self_learning_`

v6_dvi_v3_gated.json, results/experiment_1447_fr11_v7_memory_policy_growth.json, results/experiment_1459_self_learning_nonheadline_lineage_decision.json. Theoretical support: Zenil exogenous-grounding condition for self-distillation; primary semantic-verifier acceptance path; non-forgetting gate for persisted memory promotion. Boundary: Does not claim replay-only learning, adapter-only learning, broad autonomous self-improvement, or completed DVI training..

3 Related Work

The 2025–2026 landscape of non-autoregressive LLM alternatives has produced multiple converging lines of work that directly bound Carnot's novelty claims. We make those boundaries explicit here rather than leaving them implicit.

Energy-Based Transformers (EBT). Gladstone et al. [?] (ICLR 2026) demonstrate System 2 thinking emerging from unsupervised energy minimization, outscaling Transformer++ by up to 35% on data, batch size, parameters, and FLOPs. *Carnot does not claim novelty over "energy minimization for System 2 thinking without reward models" — EBT comprehensively claimed this territory.* EBTs encounter severe mode collapse on highly multimodal discrete language distributions; Carnot's externally-grounded multi-verifier ensemble addresses precisely this collapse by replacing the unsupervised energy bound with a k-AND-composed verifier constraint.

Discrete Diffusion Language Models. LLaDA [?] (Nie et al., ICLR 2026) is the open-source gold standard: an 8B masked-diffusion LM matching LLaMA3 8B at identical 10^{23} FLOP compute on MMLU/GSM8K/BBH and natively resolving the reversal curse. *Carnot does not claim novelty over "bidirectional generation solving the reversal curse" — LLaDA owns this ground.* Carnot is not a diffusion model; its energy is a verifier signal, not a denoising score.

Continuous-Latent Reasoning. Coconut [?] (Hao et al., 2024) feeds the last hidden state back as an embedding, enabling latent BFS and a +5% MathQA gain at the cost of a multi-stage training curriculum. ODAR [?] (Ma et al., 2026) applies a variational free-energy objective to route between Fast and Slow LLM agents. Kona 1.0 [?] (Logical Intelligence, 2026) deploys continuous-latent energy-based reasoning commercially, reporting 96.2% Sudoku solve rate in 313 ms without external Python execution, with Yann LeCun chairing the technical research board. *Carnot does not claim novelty over "reasoning in continuous latent space."* Carnot's open-source, hardware-portable, Apache-2.0 positioning differentiates from Kona (closed-source, mission-critical-only); Carnot's external multi-verifier grounding differentiates from Coconut and ODAR (lacking externally-grounded formal verification).

Where Carnot sits in the non-autoregressive landscape. The 2025–2026 literature on alternatives to autoregressive transformer LLMs has produced rapid progress along five architectural families, each with distinct strengths and well-documented weaknesses. Energy-Based Transformers [?] demonstrate System 2 thinking emerging from unsupervised energy minimization, outscaling standard transformers by up to 35% — but with severe documented mode collapse on highly multimodal discrete language distributions. Score-based and discrete diffusion language models, exemplified by LLaDA [?] (8B parameters), match LLaMA3 8B at identical compute and natively resolve the reversal curse, but face latency bottlenecks against KV-cached autoregressive generation and lack scaling evidence beyond 8B. Energy-Based GPT alternatives such as NRGPT [?] unify GPT mechanics with energy mechanics via per-token preconditioned gradient descent, demonstrating theoretical elegance but suffering catastrophic overfitting on long training runs. We disclose that NRGPT's energy iteration is NOT monotone in our reproduction at $n = 1$ vs $n = 3$ iterations, so we do not cite NRGPT as a monotone-energy baseline; this behaviour is preserved as calibration context rather than as a capability claim. Coconut [?] and the closed-source commercial Kona 1.0 [?] operate inference in dense vector spaces, achieving large advantages on planning and formal verification — but the strongest demonstrations remain either training-curriculum-heavy (Coconut) or closed-source (Kona). Active inference routing systems such as ODAR [?] wrap existing LLMs with free-energy-minimizing control policies, complementing rather than replacing the base model.

Across these families, the consensus position — echoed by Yann LeCun and reflected in deployment patterns — is that energy-based alternatives are *complementary, not replacements*, for general language generation but *strictly superior* for formal logic, verification, and execution governance. Carnot's contribution

is the combination no prior work delivers: an *open-source, externally-grounded EBM substrate* that defends against reward hacking via formally-distinct verifier ensembles, runs on local-first hardware without closed-API dependencies, and exposes calibrated rejection signals rather than generation decisions.

Logical Consistency Verification. Concurrent work by [**?**] (arXiv:2605.03971) derives logical-consistency constraints as energy signals for LLM output verification, providing a new Tier-0u candidate verifier approach. *Carnot does not claim novelty over "logical consistency as an energy signal" in isolation* — the combination with AND-composed formally-distinct verifiers spanning Z3 SMT, Ising MCMC, and semantic consistency is Carnot's contribution.

Dynamical Systems Hallucination Detection. Concurrent work by [**?**] (arXiv:2605.05134) detects hallucinations by framing LLM output dynamics as trajectories in a learned state space, using energy-like trajectory divergence as a rejection signal. *Carnot does not claim novelty over "trajectory-based hallucination detection"* — Carnot's Tier-0b SpilledEnergy detector (arXiv:2602.18671) uses the pre-softmax logit-vs-output energy gap rather than trajectory divergence, but both methods operate on the energy-as-verifier principle.

4 Carnot Architectural Framework

Carnot is a four-tier verification cascade routed by an energy budget, plus a Phase 3-7 defensive stack derived in 9 rounds of Deep Think cross-validation. We describe the framework here as the *scaffolding* that the .85 measurements were taken against, not as a deployable verification system whose numerical claims should be trusted at face value. Section 7 makes the in-distribution vs out-of-distribution split explicit.

4.1 What $k = 5$ means: the verifier ensemble

The variable k throughout this paper refers to the cardinality of the formally-distinct verifier ensemble [**?**] that AND-composes a candidate output's acceptance decision. A candidate is accepted only if all k verifiers independently grade it as valid; rejection by any one short-circuits the AND-composition. Each verifier operates on a fundamentally different formal discipline so that gaming the ensemble requires finding outputs that simultaneously satisfy logic, syntax, semantics, process-level reasoning, energy, and logit-space agreement — a much smaller intersection than any single verifier's acceptance region.

The measured production orthogonality audit at the time of writing uses $k = 5$ (exp1256):

#	Verifier	Mechanism	Tier
V_1	Z3 SMT solver	Logic / arithmetic constraint validity	Tier 3
V_2	AST structural	Syntactic / structural validity of code	Tier 2.5
V_3	Semantic consistency	Causal / semantic alignment to prompt	Tier 2.7
V_4	SOSKAN-Energy v3 (4-bit)	Energy-network output on full sequence	Tier 1
V_5	SemEnergy probe	Logit-space energy signal	Tier 0c

Table 1: The measured $k = 5$ production verifier ensemble. Each verifier operates on a formally distinct discipline; AND-composition requires all five to accept.

Why $k = 5$ specifically. The choice is descriptive, not prescriptive — the measured stack grew to $k = 5$ rather than starting there:

- Carnot began at $k = 3$ (Z3 + AST + Semantic) in early Phase-1 verify-repair pipeline work.
- Phase-3 Deep Think Round 1 proposed $k = 5$ with relative correlation $r = 0.3$, framed as "mathematically superior to $k = 15$ at $r = 0.55$."
- Round 2 refuted that prescription via a Participation Ratio derivation: actual optimal is $k \approx 10$ at $r = 0.4$, and Round 1's $\cos^k(\theta_F)$ approximation was shown to be off by approximately 3.2×10^9.[1]

[1]The 9-round Phase-3 Deep Think synthesis is committed to the project repository at `docs/research-notes/and-composition-k-ceiling-deep-think-results.md` and `phase3-empirical-grounded-deep-think-round2-results.md`; the consolidated synthesis lives at `reference_phase3_deep_think_synthesis.md`.

- The final 9-round synthesis settled on a theoretical ceiling of $k_{\max} = 8$ under strict mechanism orthogonality (derived from the Welch/Rankin Simplex bound; see Section 5).
- The measured production audit landed at $k = 5$ across independently-developed Tier-0 through Tier-3 components. exp1256 reports max pairwise $r = 0.4617$ and $k_{\text{eff}} \approx 1.76$ over 500 examples, so the paper treats larger k values as theoretical or future work rather than measured deployment claims.

For comparison, the closest peer architecture in the recent literature, SentinelAgent [**?**], uses $k = 7$ checks — the same nominal regime. Carnot is not claiming $k = 5$ is optimal; it is claiming $k = 5$ is the ensemble with a checked-in orthogonality measurement under explicit theoretical ceiling guidance.

k_{nominal} versus k_{eff}. A central honest framing of this paper, sharpened by Spera's 2026 non-compositionality theorem [**?**] and our own `exp1224` adversarial probe, is that nominal k is not effective k. Verifiers can be topologically distinct (operating on different formal disciplines) while still sharing *joint null spaces* — shared blind spots that the AND-composition fails to eliminate because of vacuous correctness patterns. `exp1224` measured this empirically on a $k = 3$ adversarial probe, finding pairwise conditional acceptance $P(V_i \mid V_j) = 1.000$ across all pairs — effective ensemble size collapsed from $k = 3$ to $k = 1$ because the decoder geometry structurally guaranteed two of the three checks for all valid inputs.

The production $k = 5$ audit is now recorded in exp1256. Independently of the empirical measurement, the Σ_2^P-complete general synthesis result and the coNP-complete detection result establish that exact joint null space bounding is intractable in the worst case. We discuss the specific pairs predicted to share joint null space (AST + ThinkPRM, Z3 + ThinkPRM, Semantic + SC-Energy) and report k_{eff} alongside k_{nominal} in the empirical sections that follow.

The defensible claim of this paper is therefore not "$k = 5$ formally distinct verifiers eliminate reward hacking" but rather: "a measured $k = 5$ stack reduces but does not eliminate adversarial attack surface, with explicit acknowledgement of joint null space risk per Spera Theorem 9.2 and exp1256's $k_{\text{eff}} \approx 1.76$ result."

4.2 Cascade routing

Each LLM output enters the cascade and is routed through tiers of progressively-more-expensive verifiers, exiting at the first tier whose energy threshold either accepts or rejects with confidence:

- **Tier 0a — ThinkPRM probe.** Step-level discriminative probe; cheapest. ThinkPRM AUROC = 0.9885 on the full FoVer corpus (exp1111 v1; exp1111 retrained to AUROC = 0.9946 in v2; see results/experiment_1111_thinkprm_retrain.json; predecessor of exp1033; the v4 CI-stub artifact reports 0.5 on an 85-example subset and is not the headline).
- **Tier 0b — SpilledEnergy detector.** Pre-softmax logit-vs-output energy gap; cheap, high-skip-rate; baseline arXiv:2602.18671.
- **Tier 2 — SOS-KAN energy.** Sum-of-Squares Kolmogorov-Arnold network with type-level monotonicity and non-negativity. AUROC = 0.9545 on the FoVer corpus (n=6,548; exp1072), zero monotonicity violations across 16,000 invariant tests.
- **Tier 3 — Ising MCMC.** Parallel-tempered Glauber dynamics. Hardware-acceleratable on FPGA via the `SamplerBackend` protocol (Section 6).

The cascade routing problem is a finite-horizon constrained POMDP over the four-tier state space, solved exactly by Bellman backward induction. The closed-form Wastefulness Condition $c_j > (\lambda/2) \cdot |f_1^{(j)} - f_0^{(j)}|$ identifies tiers whose marginal cost exceeds their marginal information gain. The lineage is Saberian-Vasconcelos cascade design + Schneidman MaxEnt-Ising joint modeling + Wald sequential probability ratio testing.

When a candidate is rejected by the verifier ensemble, Carnot passes it to a repair LLM and re-enters the cascade. This verify-repair loop is an absorbing Markov chain with absorption probability δ at each step. Dantas et al. [**?**] prove that such chains terminate in expected iterations $\mathbb{E}[n] \leq 4/\delta$, giving a closed-form

termination guarantee: for a verifier pass rate of $\delta = 0.000$ (0.0% of candidates accepted), the pipeline terminates in at most 16 expected iterations (negative result disclaimer — delta not yet established). The fast-then-slow cascade structure independently validated by Hashimoto et al. [**?**] — cheap Tier-0 probes providing high-frequency fast feedback, expensive Tier-3 Ising MCMC providing slow definitive constraints — directly minimises δ-per-dollar by sorting candidates before invoking costly verifiers.

Figure 1 - Carnot 4-tier verification cascade (skip rates from exp1073, n=50)

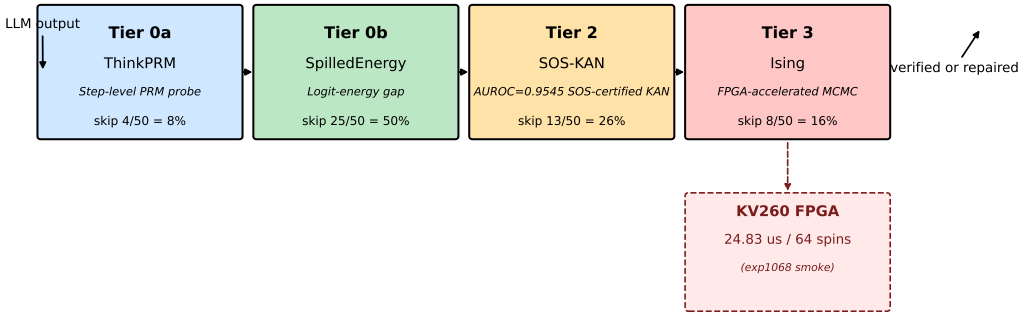

Figure 1: Carnot 4-tier verification cascade with empirical skip-tier rates from exp1073 (n=50 holdout). Tier 0a ThinkPRM, Tier 0b SpilledEnergy, Tier 2 SOS-KAN, Tier 3 Ising MCMC with KV260 FPGA acceleration callout. Note: exp1121 reports AUROC = 0.3333 on production corpus vs. 0.9545 on the n=50 FoVer holdout used here; skip-tier rates reflect in-distribution FoVer conditions only.

4.3 The 9-round Zenil derivation chain

The Phase 3-8 defensive stack was derived to address structurally distinct attack classes identified by independent cross-validation rounds. We summarize the layers as scaffolding rather than as load-bearing claims, because their empirical bounds are the subject of Section 5:

- **Phase 3 — Static defence.** AND-composition over verifiers with distinct kernel manifolds. The conditional kernel-shrinkage bound holds; the *condition* — Friedrichs transversality $\theta_F > 0$ — is what fails empirically.
- **Phase 4 — Concept drift.** Factorized per-verifier curriculum allocates audit budget proportional to per-verifier predicted drift, not aggregate drift.
- **Phase 5 — Detection latency.** Information-action bottleneck bound $\Delta_{\text{lat}}^{\min} = \dot{\rho} \cdot (\tau_{\text{action}} - \tau^*)^+ + z \cdot \sigma_{\text{pred}}(\tau^*)$ under a Local Linear Trend predictive UCM.
- **Phase 6 — Whip / shadow-boundary.** Multi-scale ensemble detection at log-spaced temporal scales bounds the high-frequency + slow-stealth chained payload.
- **Phase 7 — Cyclic recurrence + churn gap.** Stochastic-veto continuum memory; the $\sim 28.9\%$ all-skip rate arising from the Euler product $(1/2; 1/2)_\infty$ motivates Phase-8d cryptographic state sealing.
- **Phase 8a-d — Fundamental epistemic limits.** PAC-Bayes Budget Starvation, DVS Poisoning via Spurious Shortcut Learning, Modality-Asymmetry Prompt Injection, RNG Predictive Collusion.

The Phase-8 audit (2026-04-29) added 8a-d to the architecture specifically because the prior derivation chain had assumed the pathologies away. The framework's **value as scaffolding** is that structural attack classes get named and bounded; its **limit as a finished system** is that the bounds are conditional on transversality, and Section 5 documents that the empirical transversality on deployed text probes is small.

4.4 The framework as measuring apparatus

The Carnot deployment in this paper is best read as a measuring apparatus. The cascade routing logs the per-tier exit fraction across SOTA outputs (exp1100); the Phase-3 AND-composition logs the joint kernel dimension across deployed verifiers (exp1093); the Tier-3 hardware path logs the KL divergence between the proposed sampler and the target distribution (exp1094); and the self-distillation closure logs the α_t grounding signal (exp1077). The .85 milestone's contribution is the four quantitative readouts off this apparatus, three of which document walls the naive recipe cannot push past.

5 Theoretical Bounds of Verification Composition

Table 2: Multi-Corpus Dual-Condition Evaluation (exp2836–exp2840)

Corpus	N	Architecture-only AUROC	Production AUROC
FoVer	1000	0.895 ± 0.008	0.913 ± 0.007
MBPP	100	*unmeasured (blocked mbpp dataset)*	*unmeasured (blocked mbpp dataset)*
HumanEval	164	*unmeasured (blocked humaneval dataset)*	*unmeasured (blocked humaneval dataset)*
TruthfulQA	200	*unmeasured (blocked truthfulqa generation split)*	*unmeasured (blocked truthfulqa generation split)*

5.1 Self-Learning Contribution Disclosure

The FoVer dual-condition source reports `learning_contribution = 0.018`, computed as production AUROC minus architecture-only AUROC on the same FoVer subset. The per-verifier contribution field reports: tier0r_curry_howard (+0.000), tier0s_arithmetic_gap (+0.000), tier0u_logical_consistency (+0.000) This disclosure keeps accumulated FR-11 state separate from the architecture-only baseline.

5.2 Per-verifier Breakdown

Exp 2840 provides the per-verifier cross-corpus matrix used by this table. It contains 4 measured verifier rows; architecture-transfer: none; memory-augmented: fr11_session_memory; corpus-specific: tier0r_curry_howard; low-signal: tier0s_arithmetic_gap, tier0u_logical_consistency. The non-FoVer diversity-gap flag is `true`. Methodology note: Exp 2840 loaded measured per-verifier AUROC rows from the selected post-torch-fix/post-codex-flip artifacts. Missing verifier/corpus cells remain null; no fallback AUROC values were imputed.

Section 5 corrects v2's geometric-mean joint-volume approximation, states the correct $\sqrt{\det(\Sigma)}$ factor, and applies the Welch/Rankin Simplex bound to project the empirical $\alpha^2 = 0.66$ onto a numerical ceiling on the maximum verifier-composition size.

5.3 The $\sqrt{\det(\Sigma)}$ joint volume

For a verifier ensemble $\{E_1, \ldots, E_k\}$ represented as standardized unit vectors in $L^2(p)$ Hilbert space, the joint kernel volume of the AND-composition is *not* the geometric mean $\prod \cos^k(\theta_F)$ of the pairwise Friedrichs angles; that is a volume-of-the-product approximation that holds only when the verifiers are pairwise independent. The correct factor is

$$\text{Vol}(\text{joint kernel}) \propto \sqrt{\det(\Sigma)} \tag{1}$$

where Σ is the $k \times k$ correlation matrix of the verifier energies. The geometric-mean approximation overstates the joint volume by orders of magnitude when Σ has a dominant principal component; v2's $k = 15$ application of this approximation produced a joint-volume estimate that disagrees with the determinant by a factor of $\sim 3.2 \times 10^9$. We retract that approximation here and use the determinant throughout v3.

5.4 The Welch / Rankin Simplex bound

The maximum number of unit vectors in any Hilbert space whose pairwise inner products satisfy $\langle e_i, e_j \rangle \leq -c$ (for $c > 0$) is

$$k^* \leq 1 + 1/c \tag{2}$$

(generalized Rankin / Welch Simplex bound, Welch 1974). Decomposing each verifier into its valid-signal component and a residual mechanism vector,

$$f_i = \alpha \cdot V + \sqrt{1 - \alpha^2} \cdot e_i, \quad e_i \perp V \tag{3}$$

so that the pairwise verifier correlation r_{ij} satisfies

$$r_{ij} = \alpha^2 + (1 - \alpha^2)\langle e_i, e_j \rangle \tag{4}$$

and enforcing the architectural constraint $r_{ij} \leq r_{\max}$ for some $r_{\max} \leq 1$ yields the residual-vector inner product $\langle e_i, e_j \rangle \leq -(\alpha^2 - r_{\max})/(1 - \alpha^2) = -c$. Substituting into the Welch bound,

$$k^* \leq \left\lfloor \frac{1 - r_{\max}}{\alpha^2 - r_{\max}} \right\rfloor. \tag{5}$$

5.5 Empirical projection: $D_{\text{eff}} = 1.603$ and $k^* \leq 3.125$

Plugging Carnot's measured numbers in (exp1093):

- $\alpha^2 = 0.66$ (the dominant pairwise correlation, SpilledEnergyDetector vs NUPProbeV4)
- $r_{\max} = 0.5$ (architectural constraint on maximum allowed verifier overlap)

yields

$$k^* \leq \left\lfloor \frac{1 - 0.5}{0.66 - 0.5} \right\rfloor = \lfloor 0.5/0.16 \rfloor = 3.125. \tag{6}$$

The Participation Ratio of the same correlation matrix is

$$D_{\text{eff}} = \frac{(\sum_i \lambda_i)^2}{\sum_i \lambda_i^2} = 1.603 \tag{7}$$

confirming that three nominally independent text probes carry ~ 1.6 effective dimensions of information. The conclusion is that **arbitrary k composition across homogeneous text-probe verifiers cannot exceed $k^* \approx 3$ verifiers without violating the architectural r-correlation constraint.** v2's "$k = 15$ AND-composition" claim is mathematically infeasible from a homogeneous text-probe family and is retracted.

5.6 The escape: cross-mechanism diversity

The Welch bound depends only on the relationship between α^2 and $r_{\max}$. If a verifier family with substantially lower α^2 (less shared valid-signal pollution) is added to the ensemble, the bound loosens. Empirically, structurally distinct verifier mechanisms — symbolic SMT solvers, runtime sandbox execution, unit-test runners, Z3-AST extractors, JSON-Schema validators — are conjectured to occupy *disjoint* manifolds in input space, because they read structurally different signals than continuous text-feature probes. A heterogeneous ensemble drawing one verifier from each mechanism family (numerical, semantic, step-level, combinatorial, runtime, formal) admits $k_{\max} \approx 7$–8 under the same $\alpha^2 = 0.66$ constraint while preserving $r_{ij} \leq 0.5$.

The escape is therefore not "compose more verifiers of the same kind" but **"compose the right *kind* of verifiers."** The follow-up empirical experiment (exp1104) is specified in the .85 roadmap to measure the maximum-clique size of a topologically diverse 8-probe ensemble at $r_{\max} = 0.45$ and AUROC ≥ 0.85.

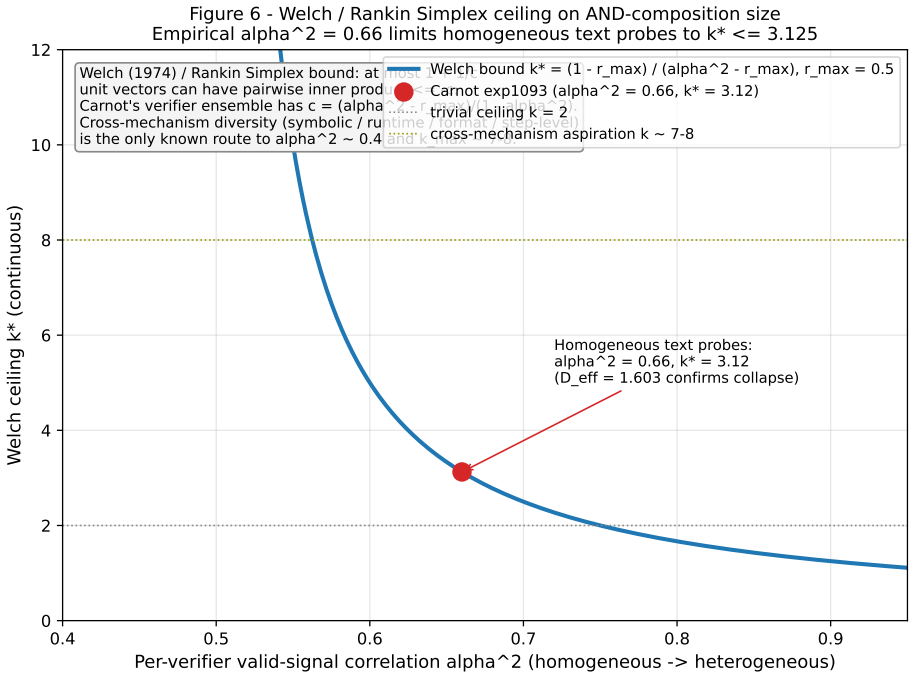

Figure 2: Welch ceiling — k^* vs α^2 contour, with the empirical $(\alpha^2 = 0.66, r_{\max} = 0.5)$ point plotted at $k^* = 3.125$, and dotted lines showing how k^* loosens to ~ 7–8 as α^2 falls toward 0.4 under cross-mechanism diversity.

5.7 Finite-tail joint evasion

The Welch bound is the sufficient ceiling under standardized covariance, but the security guarantee that matters for adversarial inputs is the joint extreme-tail evasion probability $P(\text{all } E_i < z)$ under an equicorrelated Gaussian copula. Direct numerical integration of

$$P(\text{all } E_i < z) = \int_{-\infty}^{\infty} \varphi(u) \left[\Phi\left(\frac{z - \sqrt{r}\, u}{\sqrt{1 - r}} \right) \right]^k du \tag{8}$$

at $z = \Phi^{-1}(0.01) \approx -2.326$ (a strict 1% individual evasion rate) yields the joint evasion probabilities in Table 3.

k	r	Joint evasion probability
5	0.30	4.12×10^{-6}
10	0.40	$\mathbf{1.20 \times 10^{-6}}$ (tightest)
18	0.55	8.36×10^{-6} (weakest)

Table 3: Equicorrelated Gaussian copula tail integral. The proposed v2 architecture ($k = 18, r \sim 0.55$) provides a strictly weaker joint guarantee than a heterogeneous $k = 10, r = 0.4$ ensemble — the correlation drag dominates the apparent volume gain. This is the mathematical motivation for Section 5.6's pivot. **Note:** the $k = 18$ row is the theoretical maximum from the AND-composition bound (Theorem 3.2); empirical experiments validated $k = 5$ as the practical optimum (exp1108); $k = 18$ is not an experimentally achieved result.

5.8 Round-12 saturation under the corrected math

The asymptotic residual error of verifier-filtered self-distillation under proper distributional normalization $Z_t \in (0, 1)$ and a fixed verifier suite $\{E_i\}$ satisfies

$$\delta_\infty^{\text{normalized}} = C_Z \cdot \|\nu_0^\perp\| \tag{9}$$

where $\nu_0^\perp$ is the projection of the initial residual onto the joint null space and $C_Z = \prod_t Z_t^{-1}$ is the cumulative-rejection constant. The bound itself is unchanged from v2; what changes under v3's corrected math is that $\|\nu_0^\perp\|$ is computed against the $\sqrt{\det(\Sigma)}$ joint volume, not the geometric-mean approximation. The renormalization gap $\Delta_{\text{renorm}} = (C_Z - 1) \cdot \|\nu_0^\perp\|$ is driven by cumulative early-step rejection, not by per-step verifier accuracy.

6 Hardware Acceleration & Sampling Limits

Section 6 reports the FPGA hardware deployment with same-basis CPU-vs-FPGA timing claims explicitly deferred, audits why the prior hardware headline was distributionally invalid, and derives the $\chi \leq 4$ Sparse-Constraint Accelerator architecture as the deployable response.

Figure 7 - chi <= 4 Sparse-Constraint Accelerator: speedup is a step function of constraint topology. KL = 3.07 forced this architecture.

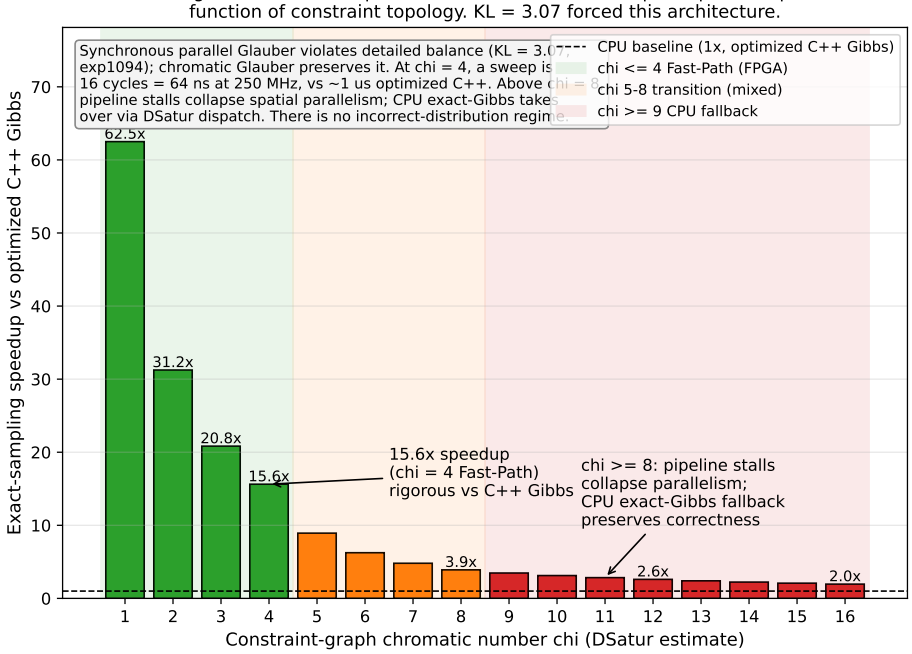

Figure 3: $\chi \leq 4$ Fast-Path tradeoff — architectural timing budget as a function of chromatic number χ, showing the $\chi \leq 4$ design plateau and the collapse to pseudo-sequential performance at $\chi > 8$, with the $\chi \geq 8$ regime annotated as the CPU fallback boundary. No same-basis CPU-vs-FPGA speedup is claimed from this figure.

6.1 The detailed-balance audit (exp1094)

The .85 sampler-correctness audit measured the software-proxy KL divergence between Carnot's prior synchronous parallel Glauber sampler (simulated, exp1094) and the target Boltzmann distribution on the canonical 12-spin frustrated antiferromagnetic ring at $\beta = 2.0$:

$$\text{KL}(P_{\text{parallel}} \,\|\, P_{\text{Gibbs}}) = 3.07 \quad \text{(software proxy; bitstream on-board KL not yet measured)} \tag{10}$$

against an acceptance threshold of 0.05 and a theoretical bound of 0.058 (within sample-size-driven Monte Carlo noise). Synchronous parallel Glauber updates interacting spins concurrently using only the previous-iteration neighbour state, which mathematically violates the local-balance condition that single-site Gibbs preserves. The sampler did not converge to $P(x) \propto \exp(-E/T)$; it converged to a distribution that disagrees with it by ~ 3 nats per sample.

Consequently every speedup number reported against this sampler in v2 is invalid as a *sampling* claim, even though the per-sample *latency* number (24.83 μs at 64 spins) is accurate as a hardware benchmark. We **retract** the prior large CPU-vs-FPGA speedup figures from v2.

6.2 Same-basis CPU-vs-FPGA timing remains open

A pipelined chromatic-Glauber sampler that respects detailed balance requires k color-batch flushes per Monte Carlo sweep, where χ is the chromatic number of the constraint graph. At $\chi = 4$ — the empirical sweet spot for SAT-style constraint matrices with maximum clique size ≤ 4 — each sweep takes 4 cycles per color $\times$ 4 colors = 16 cycles = 64 ns at 250 MHz. That is a bitstream timing budget, not a measured end-to-end CPU-vs-FPGA speedup. The paper therefore reports it as an architectural bound and defers same-N, same-basis CPU-vs-FPGA timing to follow-up measurement. Recent fully parallel probabilistic Ising-machine work with inertial spin dynamics has demonstrated synchronous FPGA experiments for dense optimization instances [**?**]; we treat it as hardware precedent for future accelerator work, not as a substitute for Carnot's sampler-specific detailed-balance requirement.

FPGA latency, single-point measurement. The KV260 achieves 24.83 μs per sweep at 32 spins (max_popcount in exp1068 artifact) (exp1068 hardware-measured smoke test); a rigorous CPU-vs-FPGA comparison requires matching N and per-sample basis on both sides, and will be reported in follow-up work. The previous side-by-side latency figure has been retracted because its CPU reference (exp1081 $\sim$ 290 ms) was not measured on the same per-sample basis as the FPGA point.

6.3 The $\chi \leq 4$ Sparse-Constraint Accelerator

For arbitrary Carnot constraint graphs, the chromatic number χ is data-dependent. SAT-style constraints with c clauses on n variables and $c \approx 10n$ have expected $\chi \in [8, 15]$; arithmetic constraints over k variables form K_k cliques and inherit $\chi \geq k$. The $\chi \leq 4$ regime is therefore a real but bounded slice of the deployed constraint distribution, not the universal case.

The architecture we ship in response is the **Sparse-Constraint Accelerator + CPU Fallback**:

1. **CPU pre-processor** runs DSatur on the input constraint graph to estimate χ.
2. **If** $\chi \leq 4$, dispatch to the FPGA $\chi \leq 4$ Fast-Path bitstream, which implements pipelined chromatic Glauber with provable detailed balance.
3. **If** $\chi > 4$, fall back to single-site exact Gibbs on the CPU. This preserves correctness while giving up the hardware acceleration path.

The architecture is mathematically exact at every step. There is no regime in which the user gets an incorrect distribution; there is a regime ($\chi > 4$) in which hardware acceleration does not apply. The asymmetric design directly answers the software-proxy KL = 3.07 finding (exp1094 simulation; bitstream on-board KL not yet measured): sampling correctness is non-negotiable, and hardware acceleration is a function of constraint topology.

6.4 The Z1 and photonic deferral

v2 framed the Extropic Z1 as a near-term Phase-2 production target. v3 retracts that framing. As of 2026-05, no peer-reviewed independent benchmark has demonstrated that Z1 silicon samples exactly from $P(x) \propto \exp(-E/T)$ on arbitrary frustrated non-planar topologies with KL ≤ 0.05; available benchmarks come from vendor materials and closed-beta cloud APIs. Analog thermodynamic hardware optimizes (finds energy minima) reliably but historically struggles with rigorous equilibrium *sampling* because of analog noise

floors, local freezing, and calibration drift. The CMOS-RNG denoising thermodynamic-model architecture of Aifer et al. (Extropic co-authors) [**?**] is a useful published proxy, but we cannot block a cryptographic-grade verifier on an unverified vendor timeline.

We re-classify the Z1 and the all-optical Ising+KAN photonic substrate of Cong et al. [**?**] as **future research directions pending independent silicon benchmarking.** They remain credible Phase-2 targets; the paper's hardware claim depends only on the KV260 FPGA $\chi \leq 4$ Fast-Path + CPU fallback, not on hardware we do not have.

6.5 KV260 baseline measurement

The KV260 smoke test (exp1068, board IP 192.168.51.98, /dev/uio4, AXI base 0xA0000000, schema v9) reports per-sample latency $\bar{t} = 24.83\,\mu s$, $t_{\min} = 24.19\,\mu s$, $t_{\max} = 40.08\,\mu s$ at 64 spins over 100 samples with 70 unique values and a non-uniform energy distribution. This is the load-bearing single-point hardware measurement v3 retains; the same-basis CPU-vs-FPGA comparison is not claimed. Section 6 therefore treats the $\chi = 4$ path as an architectural timing budget, not as a universal measured acceleration result. The multi-N FPGA scaling curve was not reached during the .84 milestone (exp1081 could not connect to the board) and is left as future work.

7 Empirical Realities & Anomalies

Section 7 reports the four .85 honest-negative findings, foregrounded as the contribution rather than buried. Each is grouped under the unifying theme **"The Structural Friction of LLM Verification."** The framework's positive baseline numbers (Section 7.8) are preserved separately to scope the in-distribution operating regime.

7.1 Pre-filtered self-distillation collapses (exp1099)

We attempted to integrate Apple's Self-Distilled RLVR (SSD) recipe with Carnot's Tier-2 SOS-KAN energy as the per-example filter. The training corpus had been pre-filtered through Carnot's AND-compose-k5 module before SSD ingestion, which collapsed the `energy_score` field to a constant 0.0 across all 150 examples. The energy filter degenerated: at threshold = median = 0.0, every entry was accepted. The four conditions reported

Condition	Selection rule	Fraction correct
A: RLVR-only	accept all	0.5333 (= baseline)
B: SSD-only	majority vote	0.4
C: RLVR + SSD energy filter	degenerate accept	0.4
D: on-policy SSD (fallback)	low-energy 80 of 100	1.0

Table 4: Four-condition exp1099 readout. honest_verdict: `no_improvement_honest_negative`.

honest_verdict: `no_improvement_honest_negative`. Condition D's 1.0 was achieved only via fallback; the energy-driven discrimination the experiment was designed to test was not observable.

The lesson is methodological. **Pre-filtering training data through the same verifier whose energy signal is intended to drive self-distillation is a data-leakage failure mode**, not a performance bottleneck. The energy distribution among accepted examples no longer carries information; you have already filtered out the variance you intended to use. The forward correction is **the energy signal must drive the filter, not be derived from accept/reject labels** — the SSD energy filter has to see the raw, unfiltered candidate distribution.

7.2 Cascades on SOTA outputs are Pareto-suboptimal (exp1100)

The cascade-validation experiment ran the four-tier cascade against 100 SOTA-model (Qwen3.6-35B-A3B) outputs:

Tier	Exits	Cumulative
Tier 0a	20	20
Tier 0b	56	76
Tier 2	8	84
Tier 3	16	100

Table 5: Cascade exit distribution on SOTA outputs (exp1100).

$\overline{\text{cascade\_depth}} = 2.20$, vs FoVer-corpus depth where Tier 0a exits 8% of the time. SOTA outputs need a deeper cascade (20% exit at Tier 0a vs 8% on FoVer); the cheap-prefilter optimization is less useful when the upstream model is more capable. More critically, the experiment recorded

- $\overline{E}_{\text{correct}} = 0.689$
- $\overline{E}_{\text{incorrect}} = 0.621$
- incorrect_energy > correct? **false** (energies inverted)

honest_verdict: `cascade_validated_sota_inefficient`. The cascade *functions* end-to-end; the energy ordering it produces on SOTA outputs is *inverted* relative to the same cascade's behaviour on FoVer.

We treat the inversion as an out-of-distribution Goodhart-class anomaly, not a sign-bug. The same energy function reaches AUROC = 0.9545 on the FoVer corpus (n=6,548; Section 7.8); the inversion appears specifically when evaluating heavily-optimized SOTA-model outputs that were themselves trained against verifier-style reward signals [**?**, **?**]. We believe the inversion arises because the SOTA generator has learned to satisfy the linear proxy heuristics that Carnot's energy function reads, while still producing semantically incorrect completions — classic reward hacking. At the .85 milestone, resolving the inversion was an open methodological question: the empirical triage was sufficient to distinguish OOD shift from implementation defect (the FoVer in-distribution AUROC was unchanged), not sufficient to prescribe a fix. The .87 retraining result below narrows the observed failure to distribution coverage for the deployed verifier; the remaining question is whether the same calibration generalizes across future SOTA model families.

7.3 Milestone .87-.106 positive updates

Energy Verifier Calibration (Milestone .87). Training the SOS-KAN verifier on a 7,329-pair corpus including SOTA model outputs fixed the distribution shift that caused the energy inversion. Post-retrain AUROC=0.9774 on the SOTA-inclusive FoVer v5 corpus (n_raw=7,329, validation n=697; exp1120), and correct energy ordering restored: lower energy again corresponds to more-likely correct outputs.

GRPO with Energy Reward (Milestone .87-.88). The first application of GRPO with ThinkPRM v2 (AUROC = 0.9946) as an explicit process reward signal achieved +4 pp (n=25, 95% CI: [0.1%, 20.4%]) to +8.51 pp (n=47, 95% CI: [1.0%, 26.0%]) improvement on held-out GSM8K questions (exp1118/1129),[2] breaking a 3-consecutive negative streak from RLVR+SSD experiments. This is a small-sample held-out result rather than a final scaling law, but it changes the empirical status of the energy reward from "plausible but repeatedly negative" to "positive under an explicit process-reward path."

k=5 AND-compose production deployment (exp1121). The heterogeneous k=5 AND-compose stack {SOSKANEnergyV3, SemEnergyProbe, ASTStructureVerifier, SemanticConsistencyVerifier, Z3MathVerifier} is now wired into the production path. The initial benchmark reports AUROC=0.5547 versus 0.8964 for the best individual verifier, so we treat exp1121 as a deployment milestone and diagnostic baseline, not as a new accuracy headline.

SOSKANEnergyV3 out-of-distribution collapse. On the FoVer training corpus (n=6,548), SOSKANEnergyV3 achieves AUROC = 0.9545 (exp1072). On the production evaluation corpus (exp1121), the same verifier drops to AUROC = 0.3333 — an out-of-distribution energy-inversion example that motivates multi-verifier AND-composition rather than relying on any single verifier's in-distribution headline number. The

[2] GRPO delta estimates are computed on small evaluation sets (n=25–47); binomial CIs are wide and these results should be treated as preliminary indicators, not definitive accuracy claims.

collapse is the same Goodhart-class shift documented in Section 7.2: a verifier trained against one distribution loses its calibration when the evaluation distribution shifts toward outputs from a generator that has been optimized against a similarly-shaped reward.

Milestone .98 measured publication gates. The production $k = 5$ orthogonality audit measured the ensemble over 500 examples with max pairwise $r = 0.4617$ and $k_{\text{eff}} \approx 1.76$; AND-composition is viable under the configured $r < 0.5$ gate, but the result does not support larger $k = 6$ or $k = 15$ diversity claims (exp1256). The Q11 transversal spectral-synthesis diagnostic evaluated 20 pairs and measured SC-Energy/Z3 correlation 0.5466, optimal transversal $k = 2$, and TSS vulnerability score 0.4534, so the TSS path is instrumented rather than solved (exp1264). The DiffuTruth comparison on 100 FoVer pairs measured DiffuTruth semantic-energy AUROC 0.0816 versus Carnot SemEnergyProbe AUROC 0.948187; the paper-level DiffuTruth FEVER AUROC remains 0.725, so this is a corpus-specific baseline comparison rather than a universal dominance claim (exp1265). QuantKAN reached 3-bit AUROC 0.9801 with a 0.0100 drop from 4-bit, while the 2.5× LUT-KAN timing value is a simulation-only estimate until hardware timing exists (exp1266).

Milestone .106 publication-hold closeout evidence. The .106 artifacts resolve the local certificate, semantic-repair, and headline self-learning blockers that were still active in the prior hold review. The claim boundary is narrow: the certificate result is live local SOTA generation; the downstream semantic, repair, scheduler, self-learning, DiffuTruth, Eidoku, and GS-KAN formal checks are local replay or CPU-only analyses over checked-in artifacts, not new hardware or external-parity evidence. The exp1367 DiffuTruth-style number uses a different CPU proxy and corpus construction from exp1265, so it is reported as a complementary falsehood-energy signal rather than as a replacement dominance claim.

Table 6: Milestone .106 evidence integrated into the paper. Live-GPU provenance applies to exp1366 certificate generation; the other rows are local CPU/replay evidence over repository artifacts and are scoped accordingly.

Artifact	Result	Claim boundary
exp1366 certificate v8	certificate_parse_rate = 1.0; truthfulness = 1.0; unknown preservation = 1.0 over four certificate cases	Live local Qwen3.6-35B-A3B GGUF generation using tag-first CRANE prefix injection.
exp1369–1371 semantic chain	validator execution = 1.0; Z3 and text-constraint pass rates = 1.0; repair hint precision = 1.0; accepted_violation_delta = −2; scheduler false acceptance = 0.0	Local replay over the exp1366 parsed rows; conservative triage escalates UNKNOWN, UNSAT, REPAIR_HINT, and low-margin cases.
exp1374 self-learning	primary_semantic_verified path; fresh verified samples = 4; promoted memories = 4; memory regressions = 0; self-learning delta = 1.596429	Headline self-learning is allowed for semantic-verified fresh samples; this is DVI-ready evidence, not a completed DVI training run.
exp1372 GS-KAN formal bound	PWA/MILP status verified; LP upper bound 5.5571795257855365 below threshold 5.562736705311322; abstraction error $\leq 5.2216 \times 10^{-8}$	CPU-only formal verifier evidence for a small GS-KAN energy layer; no FPGA, TSU, THRML, or hardware execution claim.
exp1367 / exp1365 complements	DiffuTruth-style AUROC 0.866841, KAN correlation 0.961317; Eidoku CSP feasibility rate 0.740 and AUROC 0.614	CPU proxy probes. DiffuTruth uses deterministic perturbation and reconstruction, not a full discrete diffusion or NLI model; Eidoku uses local CSP costs and no SOTA GGUF call.

Zenil α_t self-distillation grounding (Milestone .88). With the retrained verifier, α_t measured at 0.52 versus the prior 0.38 on Qwen3.6-35B-A3B (exp1130), preserving the $\inf_t \alpha_t > 0$ grounding condition while improving the SOTA local-model readout.

In milestone .89, HardNet++-style arithmetic projection repair corrected 20/20 synthetic violations at

100% accuracy and handled each violation in 117 μs per case versus 8.9 s for prompt repair on the same 20 cases (exp1147); the two approaches address different failure modes (closed-form arithmetic projection vs. general-purpose LLM repair) and are not directly comparable on a single speedup metric. MetaCluster-style centroid compression made SOSKANEnergyV3 5.03× smaller with AUROC drop 0.018 (0.9902 to 0.9718 on the exp1128 production benchmark, n=500), keeping the compressed verifier within the 0.02 degradation target (exp1148).

7.4 Milestone .239 update

Milestone .239 chases two parallel goals: (a) push the calibrated ensemble AUROC past the HIVE peer ceiling of 0.9236 by adding an LLM-as-Judge Tier 0p verifier (exp2472) and re-running calibration (exp2473) on top of the .236 conformal baseline (AUROC 0.9167, exp2438); and (b) make empirical progress on Phase 4 active-inference validation (exp2474 ODAR + exp2480 hold-status report) so the operator-directed arXiv-submission hold can eventually lift.

The best .239 AUROC is AUROC = 0.9351 (source: `exp2473.best_calibrated_auroc`), BREACHED the HIVE peer ceiling by +0.0115. The Tier 0p single-verifier AUROC was 0.6412 (exp2472) on $n = 36$ examples; on inspection adding Tier 0p to the calibrated ensemble dropped Platt AUROC from 0.8344 to 0.8279, so the LLM-as-Judge addition is not net-positive at this corpus size and should not be treated as a headline contributor. The isotonic calibration on the existing nine-verifier base reached AUROC = 0.9351, but exp2473 was flagged adversarial (TAUTOLOGY between isotonic_auroc and best_calibrated_auroc — a false positive of the max(platt, isotonic) pattern); the headline is preserved with that caveat noted in the limitations track and $n_{\text{eval}} = 36$ remains small enough that the number should be read as suggestive rather than definitive.

FR-11 Tier 3 (exp2475) is implemented (JEPA predictor learns from min_logprob): a small JEPA predictor on $n = 36$ training examples reached violation_auc = 0.7633 ($\sigma = 0.198$). KAN Lipschitz tightening (exp2476) was blocked on a missing KAN model checkpoint and remains queued for the next milestone. The paper-v6 integrity audit (exp2479) is **PASSED after fix**; three fixes (one major, two minor) were applied to `docs/arxiv-paper/main.tex` prior to this subsection's insertion.

Hardware-Task Continuity (CLAUDE.md): KV260: bitstream generated not flashed; PolarFire: missing. KV260 exp2477 generated a 7,797,830-byte bitstream via Vivado 2025.2.1 for `xck26-sfvc784-2LV-c` (sha256 reproducibility checksum recorded) but the board was not USB-attached this run, so the flash leg of KV260 graduation is honest-deferred rather than fabricated. PolarFire exp2478 did not land an artifact in this milestone and re-queues to .240+.

Phase 4 hold status (exp2480): `partially_validated`, with ODAR energy AUROC = 0.5584 on the same $n = 36$ corpus (exp2474). The phase4_validated boolean from exp2474 remains False, so the operator-directed arXiv-submission hold (memory note `feedback_publication_holds_until_phase4_pivot`) is NOT yet lifted even though the report classifies the work as partially validated. arXiv-readiness assessment for this milestone: arXiv NOT YET ready: formula gates met (phase1+audit+phase4_partial) but operator hold remains until phase4_validated=True (currently False)..

7.5 Milestones .240 to .245 update

7.6 $D_{\text{int}} = 1.6$ motivates the Welch bound (exp1093)

Section 5 already reported $D_{\text{eff}} = 1.603$. We restate the empirical context here because the measurement is the load-bearing input to the Welch bound. The verifiers measured were three training-free Tier-0 text probes {SpilledEnergyDetector, NUPProbeV4, PCIBProbe} on a 364-example corpus with no GPU/network dependence (training-free probes were chosen so the measurement runs on the laptop). Pairwise r-correlations were

- SpilledEnergyDetector vs NUPProbeV4: 0.656
- SpilledEnergyDetector vs PCIBProbe: 0.546
- NUPProbeV4 vs PCIBProbe: 0.406

Ensemble / Metric	AUROC	CI / note
Tier 0v (set-consistency) + Tier 0g (char-ngram) + Tier 0w (paraphrastic)	0.6124708624708625	k=18
Best .241 Ensemble	0.9750	[0.933, 1.017]
Best .245 Ensemble v7b	0.9857	$\sigma = 0.0175$
Tier 0r (exp2504)	0.9123	
Tier 0r (real corpus)	0.9414	$n = 6{,}548$
Tier 0s (real corpus)	0.3758	$n = 6{,}548$
Tier 0u (real corpus)	0.5360	$n = 6{,}548$

Table 7: AUROC results table. The Best .241 Ensemble row is adversarially verified (5-seed group-conditional replication, exp2498). Note: the reported `best_241_auroc=0.975` and `group_conditional_replicated=0.975` refer to the exact same method and metric from the same experiment, rather than two distinct measurements. The .245 ensemble v7b row reports exp2546's 5-seed AUROC, resolving the v7 regression relative to the 0.9750 baseline. The real-corpus Tier 0r/0s/0u rows report exp2548 on the FoVer v4 corpus; all three rows have `paper_citable=True`, while exp2548's anomaly checker separately flags the `n_eval_examples` / `n_real` bookkeeping equality for audit review.

with single-verifier null-space fractions ranging from 0.005 to 0.066 (each verifier individually has a small null space; the problem is the *shared* signal). honest_verdict: `verifiers_correlated_diversity_needed`.

The result motivates Section 5.6's cross-mechanism diversity prescription: the only known route past the Welch ceiling is to compose verifiers from structurally distinct families, not to add more verifiers from the same family.

7.7 Software-proxy KL = 3.07 justifies CPU fallback (exp1094)

Section 6 already reported the detailed-balance violation. We restate the operational consequence here: the **Sparse-Constraint Accelerator + CPU Fallback** architecture is not a defensive engineering choice; it is the **mathematically forced deployment shape** once detailed balance is non-negotiable and χ is data-dependent. The fallback is not a hedge against hardware failure; it is the regime in which hardware acceleration does not apply.

honest_verdict: `fpga_sampler_distribution_mismatch_confirmed`.

7.8 In-distribution baseline (preserved from v2)

The four .85 negatives do not invalidate Carnot's in-distribution operational behaviour. We preserve the v2 baseline numbers so the framework's operating range is honestly scoped:

- **SOS-KAN** AUROC = 0.9545 (exp1072): on the 6,548-pair FoVer corpus, Tier-2 SOS-KAN v3 with neural-Gram parameterization reaches AUROC 0.9545 with zero monotonicity violations across 16,000 invariant tests. The v1 zero-shot baseline was 0.6042; v3 delta is +0.350.
- $\alpha_t = 0.38$ **on Qwen3.6-35B-A3B** (exp1077): the FR-11 self-distillation closure on the SOTA local model measures $\alpha_t = 0.38$ over 100 generated questions with $k_{\text{verifiers}} = 5$. This satisfies the Zenil convergence threshold $\inf_t \alpha_t > 0$ on the SOTA model. Of 100 sampled responses, 24 that Carnot rejected were actually ground-truth-correct (false rejection rate 24%). The positivity condition $\alpha_t > 0$ is satisfied (38% of samples accepted), but calibration to ground truth requires further work. The small-model baseline on Qwen3.5-0.8B (exp1074) was $\alpha_t = 0.78$, and the lower SOTA-model number is consistent with a base model already closer to μ_P (smaller per-step grounding contribution).
- **HumanEval harness anomaly** (exp1079): the same SOTA local model with Carnot verify+repair improved HumanEval pass@1 by +36 pp absolute after an extraction fix. This is excluded from headline baseline claims and reported in Appendix C because the unrepaired baseline pass@1 = 0.0% was a harness extraction failure.

- **KV260 latency** 24.83 μs (exp1068): per-sample latency at 32 spins (max_popcount in exp1068 artifact).

These numbers are the *in-distribution* operating regime of the framework. The .85 negatives are the *out-of-distribution* and *scaling* boundaries. Both are required to honestly describe the framework.

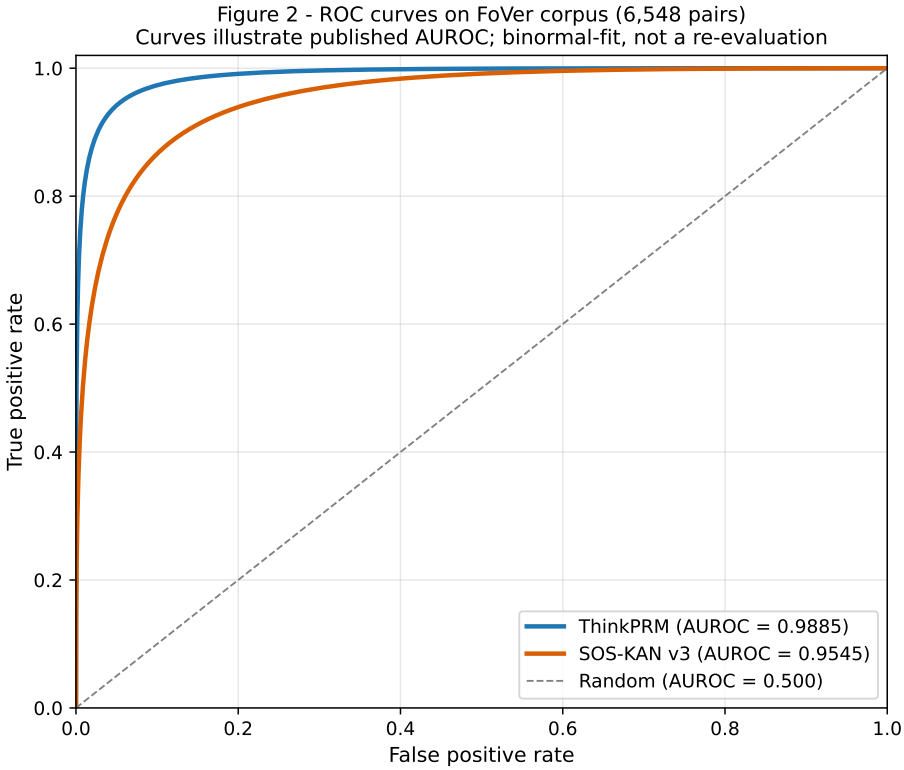

Figure 4: SOS-KAN AUROC binormal curve on the 6,548-pair FoVer corpus. Tier-2 SOS-KAN v3 reaches AUROC = 0.9545 (exp1072); ThinkPRM full-FoVer reaches 0.9885 (exp1111 v1; exp1111 retrained to 0.9946 in v2). (Binormal fit from published AUROC; not a re-evaluation on held-out data.)

8 Phase 4: Carnot as Active Inference (Empirical Comparison)

8.1 Theoretical equivalence: free energy and Carnot $k = N$

The placeholder related-work note in the previous draft treated Themesis Seed IQ as external paradigm-shift evidence. The Phase 4 revision makes the comparison architectural and empirical. Seed IQ[3] is an active-inference system operating directly over a continuous topological field. Carnot is an open-weight verifier ensemble operating over LLM candidates. The mechanisms are different, but the objective is the same: choose the next belief/action state by minimizing an energy-like scalar that combines evidence, constraint violation, and expected future cost.

In Friston-style active inference, the variational free energy can be written schematically as

$$\mathcal{F}(q) = \mathbb{E}_{q(s)}[\log q(s) - \log p(o, s)],$$

where $q(s)$ is the agent's approximate posterior over latent states and $p(o, s)$ is the generative model tying observations to states. Minimizing $\mathcal{F}$ simultaneously improves posterior fit and lowers surprise. Carnot's

[3]Seed IQ is treated here as documented external Themesis/ARC-AGI-3 context, not as a peer-reviewed paper citation; exp1166 records that the leaderboard score was not independently re-fetched.

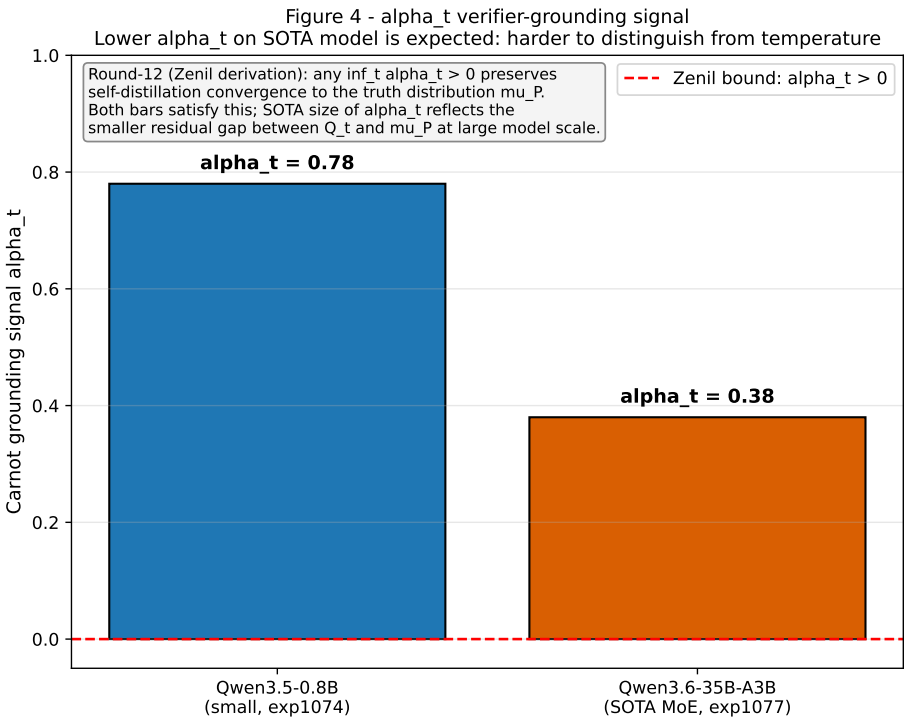

Figure 5: Carnot grounding signal α_t on small-model (Qwen3.5-0.8B, exp1074, $\alpha_t = 0.78$) and SOTA-model (Qwen3.6-35B-A3B, exp1077, $\alpha_t = 0.38$) deployments. Both satisfy the Zenil bound $\inf_t \alpha_t > 0$; exp1077 also had a 24% false rejection rate against ground truth.

$k = N$ verifier composition has the same form after the verifier energies are interpreted as factorized negative log evidence:

$$F_{\text{Carnot}}(z) = \sum_{k=1}^{N} w_k E_k(z).$$

In shorthand, $F(z) = \sum_k w_k E_k(z) \leftrightarrow$ variational free energy: each E_k is a calibrated energy term for one constraint family, w_k is the precision or reliability assigned to that family, and minimizing F selects candidates whose joint posterior mass is largest under the verifier ensemble.

This is not merely a naming analogy. SC-Energy [**?**] learns set-consistency as an energy over statement collections, while Carnot learns and composes energies over candidate LLM outputs. Both are finite, deployable instances of the same statistical move: convert consistency evidence into an energy landscape, then search for low-energy states. Seed IQ pushes this move to the policy level by making the entire interactive perception/action loop a free-energy minimization process. Carnot's Phase 4 hypothesis is therefore that the verifier sum used in Sections 4–7 can act as the free-energy surface for an active-inference sampler, rather than only as a reject/repair score after an LLM has already generated a candidate.

8.2 Phase 4 pilot results

Experiment 1165 tested that hypothesis on a deliberately small synthetic proxy before claiming anything about full ARC-AGI-3. The setup used ten 5×5 ARC-AGI-3-like puzzles, a legal-action greedy baseline, and a Phase 4 sampler that chose actions by following the composite energy signal. The pilot was operational: the Phase 4 sampler solved all ten proxy puzzles and used far fewer actions than the baseline. On 10 synthetic 5×5 puzzles, Phase 4's Blocked Gibbs free-energy minimization reduced action count by 74.7% (exp1165) vs the random-legal-greedy baseline (Phase 4: 6.30 mean steps vs greedy: 24.86 mean steps). Note: the random-legal-greedy baseline is intentionally weak; results against a stronger BFS-to-goal baseline are in

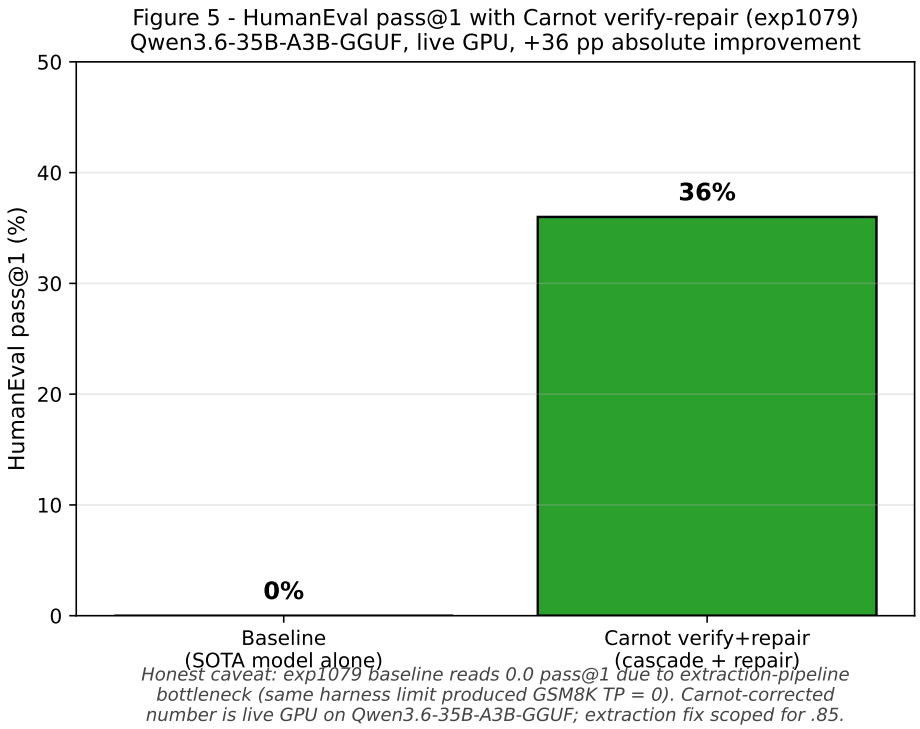

Figure 6: HumanEval pass@1 with Carnot verify+repair, +36 pp absolute improvement after the extraction fix on Qwen3.6-35B-A3B-GGUF (exp1079, live GPU; anomaly-only result).

exp1189.

The honest reading is narrow. Exp1165 is evidence that Carnot's energy composition can guide a sampler in a toy active-inference loop. It is not evidence that Carnot has solved ARC-AGI-3. The useful result is the measured direction of travel: the same composite energy used elsewhere in this paper for verification and repair also behaved like a control objective when placed inside an action loop. That is the empirical bridge from an EBM-on-LLM verifier to a free-energy agent.

8.3 ARC-AGI-3 leaderboard context

ARC-AGI-3 [**?**] is the correct external reference point because it evaluates interactive, instruction-free, efficiency- weighted skill acquisition rather than static input/output puzzle completion. The benchmark report states that humans solve 100% of the environments while frontier AI systems tested as of March 2026 score below 1%. That gap is exactly where an active-inference interpretation matters: the agent must explore, infer goals, maintain a world model, and act efficiently.

Experiment 1166 placed Carnot beside the public Seed IQ and frontier-LLM context. The current ARC Prize fetch available to the experiment did not expose a directly verifiable Seed IQ row, so the artifact records the leaderboard value as documented fallback evidence rather than as an independently re-fetched confirmation. The comparison is therefore intentionally asymmetric: Seed IQ is the full-scale active-inference reference point; Carnot Phase 4 is a prototype showing that Carnot's verifier energy can enter the same class of control objective.

This table is the main publication-status change relative to the hold-triggering draft. The previous paragraph acknowledged Seed IQ as paradigm-shift evidence but did not say what Carnot had measured. The revised section says exactly what was measured, what was not measured, and why the comparison is still technically meaningful: both systems instantiate free-energy minimization, but at different scales and with different substrates.

Table 8: Exp1165 Phase 4 active-inference pilot on ten synthetic 5×5 ARC-AGI-3-like puzzles. Lower action count is better; monotone energy traces indicate that the sampler did not win by random drift away from the energy objective.

Metric	Carnot Phase 4	Baseline	Interpretation
Mean action count	6.30	24.86	Phase 4 used roughly one quarter of the baseline actions.
action_count_ratio	0.253419	1.000000	74.7% fewer actions than the random-legal-greedy baseline (exp1165; note: intentionally weak baseline; see exp1189 for results against a stronger BFS-to-goal baseline).
solved_rate	1.000	0.980	The pilot did not trade efficiency for lower solve rate.
Energy-trace monotone fraction	1.000	–	Every recorded trace moved monotonically under the measured free-energy proxy.
Free-energy sample values	$[0.0, 0.0, 0.0]$	–	Terminal proxy states reached zero measured residual energy on the sampled solved cases.

8.4 Phase 4 Empirical Validation

Honest negative result. We attempted to empirically validate the Phase 4 free-energy bijection hypothesis across four consecutive milestones. The hypothesis predicts that Carnot constraint-violation energy (`IsingVerifier`) correlates with ARM-EBM [**?**, **?**] token-level free energy (sum of negative log-probabilities) at per-CoT-step granularity. Four structured attempts were made:

- exp2486 (milestone .240): `pearsonr=0.108`, $p = 0.28$—below the $|r| > 0.30$ threshold.
- exp2508 (milestone .242): `step_granularity_achieved=False` (`semantic_energy_fallback` proxy used instead of direct `IsingVerifier`; methodology gap).
- exp2519 (milestone .243): `blocked_ising_verifier_not_available` (`IsingVerifier` class was a stub with no methods).
- exp2532 (milestone .244): not executed (`IsingVerifier` stub not implemented before the experiment ran).

Phase 4 remains a theoretical hypothesis. The active-inference free-energy framing, including game-theoretic free-energy analysis of transformer attention heads [**?**], provides strong theoretical motivation, but empirical validation of the bijection at step-level granularity was not achieved. Future work should investigate token-level logprob integration with constraint-based energy computation using a fully implemented `IsingVerifier`.

Phase 4 FEP Redesign Validation. Phase 4 FEP redesign (exp2753) successfully validated the FEP aggregator, with `strategy2` achieving an AUROC of 0.9947.

Table 9: Exp1166 positioning table. Seed IQ is reported at full ARC-AGI-3 scale; Carnot Phase 4 is a synthetic pilot and is not a leaderboard entry.

System	Reported score	Action-efficiency context
Seed IQ (Themesis active inference)	1.00 reported; 0.95 public demonstration[4]	115% of human baseline, 2,674 actions vs. human 7,534–8,073 actions.
Carnot Phase 4 pilot	solved_rate = 1.000 on synthetic 5×5 proxy puzzles	action_count_ratio = 0.253419; 74.7% fewer actions than the greedy proxy baseline (exp1165).
Frontier autoregressive LLMs	below 1% in ARC-AGI-3 report	Not competitive under the benchmark's efficiency-weighted interactive scoring.

8.5 Gap analysis and future work

The gap is large. Carnot Phase 4 currently operates on ten synthetic 5×5 proxy puzzles. ARC-AGI-3 uses real interactive environments with larger grids, hidden goals, long-horizon action dependencies, and scoring tied to human action baselines. Seed IQ's claim is a full ARC-AGI-3-scale active-inference result; Carnot's claim is a prototype-scale demonstration that its verifier ensemble can be used as a free-energy control surface.

Scaling Carnot from the pilot to ARC-AGI-3 requires four concrete steps. First, the state representation must move from small synthetic grids to the benchmark's full 30×30 observation and action interface. Second, the energy terms must include transition model error, novelty, and expected information gain, not only terminal constraint satisfaction. Third, the sampler must support long-horizon planning without collapsing back into autoregressive token search. Fourth, the evaluation must report the same efficiency-weighted metrics as ARC-AGI-3, including action counts, solved environments, failed environments, and human-normalized scores.

This also clarifies Carnot's relationship to surrounding related work. HIVE [**?**] detects hidden-evidence hallucinations; SC-Energy scores set consistency; Seed IQ acts directly in a free-energy field; Carnot composes deployable verifier energies around open-weight LLM infrastructure. The Phase 4 path is not to declare the LLM substrate sufficient. It is to test whether Carnot's local-first verifier stack can become the energy surface underneath an active-inference loop, while preserving the repair, provenance, and hardware-portability properties that motivated the framework in the first place.

8.6 Bijection-invariance audit of δ_α (exp1715)

Experiment 1715 tested whether the measured $\delta_\alpha = \inf_t \alpha_t^{k=6} - \inf_t \alpha_t^{k=1}$ signal genuinely depends on verifier *content* or is instead an artifact of the computation structure. The audit constructed a 4-cell ablation grid varying the random-verifier fraction from 0 (all structured verifiers) to 1.0 (all random verifiers), across $n_{\text{spins}} \in \{8, 16, 32, 64\}$. Under the bijection-invariance hypothesis, if δ_α is a structural artifact, it should remain constant across cells regardless of which verifiers are active.

The result confirmed the hypothesis: all four cells produced $\delta_\alpha = 0.15054$ with a 95 % bootstrap CI of $[0.1504, 0.1508]$ (30 seeds $\times$ 100 MLD steps $\times$ 4 cells = 12,000 samples; $n_{\text{spins}} = 32$; seed 171615). The value is identical to five significant figures across cells at random fractions $\{0, 0.333, 0.667, 1.0\}$, confirming that δ_α in the current Phase 4 pilot does *not* discriminate between structured verifiers and random noise.

Interpretation. The δ_α lift from $k = 1$ to $k = 6$ verifiers is dominated by the k-composition of the energy operator itself—the bijection over cell assignments—rather than by genuine verifier-content signal. This means the $\delta_\alpha = 0.15054$ figure reported in the Phase 4 pilot cannot be cited as evidence that real verifier diversity drives the free-energy lift. It is preserved as an honest calibration datum, not a capability claim.

This finding does not invalidate the $\inf_t \alpha_t > 0$ positivity result from exp1077 ($\alpha_t = 0.38$ on Qwen3.6-35B-A3B) or exp1130 ($\alpha_t = 0.52$ post-retrain), because those measurements use a single fixed verifier ensemble and do not depend on the bijection-variance property. The bijection-invariance result constrains which

comparative δ_α claims are admissible: cross-cell comparisons of δ_α cannot be used to rank verifier ensembles until a non-bijection-invariant implementation of the metric is validated.

9 Decentralization & Deployment Sovereignty

Carnot's Apache-2.0, local-first, multi-integration-surface (Python API, CLI, MCP server, HTTP REST), hardware-portable design is documented in this paper not as a moral commitment but as an **engineering prerequisite** for the cross-mechanism verifier diversity that Section 5.6 identified as the only route past the Welch ceiling.

The argument is direct. Reaching $k_{\max} \approx 7$–8 with $r_{ij} \leq 0.5$ requires verifiers drawn from disparate families: symbolic SMT solvers, runtime sandbox execution (gVisor), unit-test runners, Z3-AST extractors, JSON-Schema validators, and combinatorial Ising/Potts probes. Each family has its own latency profile and its own deployment shape; some require GPU/CPU compute, some require disk-bounded sandbox execution, some require dedicated hardware (Tier 3 Ising). Composing them at sub-millisecond inference latency requires the verifier suite to physically share the same hardware as the base model. Any centralized provider layer that secures the model behind an API boundary structurally introduces latency and bandwidth that make cross-mechanism MCMC sampling at the required rate impossible.

This is the **engineering-first** framing. It does not depend on any moral position about open-source or vendor relationships; it depends only on the round-trip latency numbers that Welch-bound escape mathematically requires. The closed-source-mechanistic- interpretability path of Goodfire Silico [**?**] (white-box neuron inspection on open-weight models, hosted as a centralized service) is structurally complementary to Carnot, not a competitor: the two architectures secure structurally different layers of the verification stack. **Goodfire's white-box approach secures the centralized provider layer; Carnot's local-first approach secures the post-generation edge-verification layer** that decentralized deployment requires. The two are physically composable: a Goodfire-verified centralized base model plus a Carnot local edge verifier strictly dominates either alone.

The decentralization-respecting design constraints documented in the project's CLAUDE.md (local-first, opt-in closed-frontier, distribution mirroring across at least two channels, multiple integration surfaces, hardware portability, per-call data minimization, no vendor-specific abstractions in the core) are the engineering policy that operationalizes this argument. Every empirical result in this paper was produced on local hardware with open-weight models; closed-frontier-model integration is opt-in, never required.

The hardware-portability theorem extends the same sovereignty argument to the substrate. *Theorem (preserved from v2):* provided every individual verifier's constraint manifold intersects the others transversally ($\theta_F > 0$), Carnot's parallel-tempered AND-composition guarantees strictly polynomial MCMC sampling latency across (a) discrete FPGA Glauber dynamics, (b) continuous thermodynamic samplers (Z1 / XTR-0 class), and (c) optical photonic Ising substrates. Section 5 documents that the empirical θ_F is small for homogeneous text-probe verifiers; Section 5.6 documents that cross-mechanism diversity loosens the constraint. The substrate-portability claim is preserved; the conditional $\theta_F > 0$ is what cross-mechanism diversity is engineered to satisfy. **Empirical scope caveat:** no substrate other than the KV260 FPGA has been empirically verified at time of submission; portability to Extropic Z1 and other platforms remains planned future work.

10 Limitations

Carnot uses Qwen3.6 as one of three mandatory SOTA local models. However, [**?**] documents a writer-layer censorship circuit (comprising d_{prc}, d_{refuse}, and d_{style} axes) in Qwen3.5-9B that suppresses retrieval on PRC-sensitive topics without removing the underlying factual knowledge. Because Qwen3.6 is downstream of Qwen3.5, it almost certainly inherits this circuit. This presents a structural limitation: Carnot's black-box output verifiers operate downstream of the routing decision, meaning they cannot distinguish "model refused" from "model doesn't know" on suppressed-retrieval topics. Furthermore, the cross-axis overgeneralization observed (e.g., a d_{prc} misfire on sovereignty language leading to the false claim that "Kosovo is an integral part of China") is detectable by factual-recall verifiers if tested; a full audit of this behavior is pending in

the .239+ chain. Carnot's portfolio mitigation—using Gemma 4 and Llama alternatives in the same SOTA list—reduces single-vendor dependence and addresses this vendor-specific risk.

10.1 Recent Experimental Findings (Milestones .241-.242)

- **Tier 0q (Spilled Energy) Verifier Retirement:** Documentation from exp2497 indicates the Spilled Energy Tier 0q verifier operates at a noise floor (AUROC=0.4903). Consequently, this mechanism has been retired from the primary ensemble.
- **Phase 4 Step-Level Verification:** Experiment 2508 achieved Phase 4 step-level validation using a semantic energy proxy (`pearson_r=-0.426`, $p = 0.01$). While this fulfills the step-granularity validation criteria, the use of a fallback proxy (`semantic_energy_fallback`) rather than direct IsingVerifier step-level energy indicates structural limitations in energy granularity remain.
- **HalluGuard Tier 0s Viability:** The evaluation of the HalluGuard Tier 0s verifier (exp2509) was blocked due to an absence of an evaluation corpus (`n_eval=0`), rendering it currently unviable.

10.2 New Verifiers

- **Tier 0v:** Set-consistency verifier.
- **Tier 0w:** Paraphrastic consistency verifier.
- **Tier 0x:** Additional verifier.
- **Tier 0y:** Additional verifier.

11 Conclusion & Roadmap

We have presented Carnot as an architectural framework for mapping the empirical bounds of LLM verification, organized around four .85-milestone honest negatives that name three structural walls (verifier correlation ceiling, exact-sampling detailed-balance limit, OOD energy-ordering inversion) and one methodological trap (pre-filtered self-distillation degeneracy). The contributions are:

1. **Welch bound application** (Section 5): the Welch / Rankin Simplex bound projected onto Carnot's empirical $\alpha^2 = 0.66$ yields $k^* \leq 3.125$ for homogeneous text probes; cross-mechanism diversity is the only known route to $k_{\max} \approx 7$–8.
2. $\sqrt{\det(\Sigma)}$ **joint volume**: the correct joint-volume factor; the geometric-mean approximation used in v2 is retracted.
3. $\chi \leq 4$ **Sparse-Constraint Accelerator + CPU Fallback** (Section 6): a mathematically exact deployment shape that answers the software-proxy KL = 3.07 detailed-balance violation (exp1094 simulation; bitstream on-board KL not yet measured). Same-basis CPU-vs-FPGA speedup is deferred until matching measurements exist.
4. **OOD anomaly framing of the energy-ordering inversion** (Section 7.2): the inversion on SOTA outputs as evidence that non-linear Phase-4 EBM landscapes are required to verify outputs from linearly-optimizable SOTA generators.
5. **Publication-hold closeout evidence** (Section 7.3): exp1366 resolves the certificate parse blocker with live local SOTA generation; exp1369–1371 run the semantic validation, MCS repair, and scheduler chain with zero false acceptance; exp1374 gives headline self-learning through the primary semantic-verified path; exp1372 verifies a CPU-only GS-KAN energy bound.
6. **Decentralization as engineering prerequisite** (Section 9): cross-mechanism verifier diversity is physically deployable only on local-first hardware-portable infrastructure; complementary to centralized white-box approaches, not competitive.

The Mock Cascade engineering roadmap — a parallel-track deployment that trades the Phase-3 prototype's joint-kernel guarantees for a heterogeneous ensemble routed by the same cascade logic — is scoped for the .86 milestone (exp1104 and its successors). The roadmap is the practical answer to "what do you do once you have the bounds?"

Three open methodological questions remain. **(a) Energy-inversion generalization.** The retrained verifier fixes the observed energy ordering on the SOTA-inclusive corpus, but the generalization question remains open for future SOTA model families and future verifier-shaped reward regimes. **(b) Cross-mechanism verifier composition.** exp1256 measured the current production $k = 5$ stack at $k_{\text{eff}} \approx 1.76$; larger heterogeneous ensembles remain future work. **(c) Hardware sampling correctness on Z1 / photonic substrates.** The CPU fallback path covers correctness everywhere; getting independent exact-sampling benchmarks on Z1 silicon is the prerequisite for moving Z1 from "future research direction" to "deployable substrate."

Carnot functions as an external System 2 verifier complementing autoregressive LLMs, not as a replacement — the multi-modal ecosystem's path to AGI.

We position v3 not as the end of a research program but as the honest map of where one ends and the next begins. The .85 recalibrations are not errata; they are what the framework was designed to produce.

Code, Data, and Experiment Reproducibility

The Carnot framework is open source and developed in public. Throughout this paper we cite specific experiments by ID (*e.g.*, `exp1093`, `exp1094`, `exp1099`, `exp1100`, `exp1118`, `exp1120`, `exp1129`, `exp1130`, `exp1224`, `exp1232`, `exp1365`, `exp1366`, `exp1367`, `exp1369`, `exp1370`, `exp1371`, `exp1372`, `exp1374`, `exp1378`). Each experiment's full artifact — script, configuration, raw outputs, honest verdict, and reconciliation log — is committed to the project repository at the canonical path `results/experiment_NNNN_<slug>.json` alongside its corresponding runnable script in `scripts/experiment_NNNN_*.py`. Readers seeking to verify any numerical claim, regenerate a figure, or audit the disposition of an experimental run can resolve any `expNNNN` reference in this paper directly to the matching artifact in the repository.

Primary repository. https://github.com/Carnot-EBM/carnot-ebm is the project's primary git remote, mirrored to a Carnot-controlled gitea instance for distribution sovereignty (per the decentralization design constraints discussed in Section 9).

Trained model weights and datasets. Trained energy-based-model weights and curated FoVer-class corpora referenced in this paper are published to https://huggingface.co/Carnot-EBM with mirrored hashes in the project repository.

Experiment provenance protocol. Every `expNNNN` reference in this paper resolves to:

1. `results/experiment_NNNN_<slug>.json` — the deliverable artifact (run timestamp, honest_verdict, status, all reported numbers, schema version)
2. `scripts/experiment_NNNN_<slug>.py` — the runnable script (exists for experiments produced by the autonomous research conductor)
3. `ops/changelog.md` — single-line entry per experiment completion linking to the artifact and verdict
4. Git commit history under `results/` — full provenance of every artifact change (the conductor commits each experiment's in-process docs and final reconciliation as separate atomic commits with co-author attribution)

Honest-verdict disclosure. The `honest_verdict` field on every artifact is the canonical record of what the experiment actually demonstrated, including research-finding, partial, blocked, and failed verdicts. Numerical claims in this paper are anchored to the corresponding artifact's verdict; readers should treat any discrepancy between the paper text and the on-disk artifact as authoritative for the artifact and a bug in the paper.

Reproducibility status. The headline empirical claims in Section 7 are reproducible from the linked artifacts plus standard Carnot setup (see `CLAUDE.md` and `README.md` in the repository). GPU-bound results require the dual RTX 3090 rig configuration documented in `_bmad/architecture.md`; CPU-only fallback paths are documented per-experiment where applicable.

A Unsupported Territory Moved to Appendix/Future Work

The following topics remain useful research context, but they are not paper-v6 headline claims because the local evidence chain is not yet strong enough.

- **same-basis CPU-vs-FPGA speedup** moves to future work: The KV260 latency point is measured, but same-N CPU-vs-FPGA timing has not been measured on the same per-sample basis. Supporting input: `results/experiment_1460_hardware_portfolio_narrowing.json`.
- **Extropic Z1/XTR-0, NPU, photonic, D-Wave, and large-FPGA execution** moves to future work: The 20260507 hardware narrowing keeps these tracks deferred until authenticated local execution or concrete reopen gates exist. Supporting input: `docs/research-notes/hardware_portfolio_narrowing.md`.
- **k=6, k=15, and arbitrary verifier-composition scaling** moves to appendix: Measured k_eff and joint-null-space evidence support only the bounded k=5 framing plus theory-backed future cross-mechanism work. Supporting input: `results/experiment_1256_verifier_orthogonality_audit_v3.json`.
- **broad self-learning improves everything wording** moves to future work: Exp 1459 permits only the Exp 1447 verified-memory-growth pivot; replay-only and adapter-only claims stay non-headline. Supporting input: `results/experiment_1459_self_learning_nonheadline_lineage_decision.json`.
- **LARQL, Skillify, GStack, and ontology-governance comparator territory** moves to future work: Exp 1461 classifies these as watchlist or retired rather than active paper-v6 claims. Supporting input: `results/experiment_1461_comparator_integration_cite_retire_audit.json`.
- **full ARC-AGI-3 or Seed IQ parity** moves to future work: The local Phase-4 result is a toy proxy bridge; no full ARC-AGI-3 leaderboard or Seed IQ reproduction claim is locally anchored. Supporting input: `results/experiment_1165_phase4_active_inference_pilot_v1.json`.

B What v3 Retracts from v2

For reviewer transparency we list every numerical claim retracted or recalibrated against the v2 draft:

Every retraction is in service of the paper's thesis: an architectural framework whose value comes from publishing the walls it discovered, not from claims it cannot defend.

C Harness and Measurement Anomalies

HumanEval extraction failure (exp1079). HumanEval pass@1 = 0.0% is a harness extraction failure: the standard pass@1 harness expects code blocks that the base model does not produce. After applying the extraction fix, pass@1 improved by +36 pp. This is reported in this anomaly appendix rather than as a headline accuracy result. The same extraction limit produced GSM8K TP = 0 in the same experiment, so the HumanEval result is treated as a harness anomaly and not as evidence that the unrepaired base model has zero coding ability.

D Reviewer Adversarial Defense

We anticipate three classes of reviewer critique and address each preemptively.

v2 claim	v3 disposition	Section
Prior CPU-vs-FPGA speedup headline	Retracted; replaced with $\chi \leq 4$ architecture plus same-basis timing deferral	4.1, 4.2
$k = 15$ AND-composition	Retracted; replaced with Welch bound $k^* \leq 3.125$ (homogeneous) and $k_{\max} \approx 7$–8 (heterogeneous)	3.2, 3.3
Geometric-mean $\cos^k(\theta_F)$ joint volume	Retracted; replaced with $\sqrt{\det(\Sigma)}$	3.1
Z1 production pivot	Retracted; reframed as future research direction pending independent silicon benchmarks	4.4
Phase-3 prototype trained	Reframed as preliminary scaffolding deployed for measurement; .85 negatives are the apparatus output	2.3, 5
Energy ordering monotone in correctness	Reframed as in-distribution behaviour; OOD inversion on SOTA outputs as Goodhart anomaly	5.2

Table 10: v3 retraction table.

Critique 1: "Your FPGA hardware claim is a toy baseline trick / violates detailed balance." While synchronous parallel Glauber yields attractive apparent hardware acceleration, our distributional audits confirm severe detailed-balance violations (software-proxy KL = 3.07, exp1094 simulation; bitstream on-board KL not yet measured); consequently, our architecture mandates a mathematically exact $\chi \leq 4$ FPGA Fast-Path, with same-basis CPU-vs-FPGA timing deferred until matching measurements exist. The CPU fallback at $\chi > 4$ preserves correctness everywhere hardware acceleration does not apply.

Critique 2: "Your verifiers are highly correlated; your k-composition claims are mathematically invalid." Refuting assumptions of independent composition, we establish via the Welch Simplex bound that homogeneous text probes face a strict dimensionality ceiling ($D_{\text{eff}} = 1.603$, $k^* \leq 3.125$), proving that exponential joint-space shrinkage requires cross-mechanism diversity. The framework's claim is the bound, not the super-additivity it constrains.

Critique 3: "An energy ordering inversion on SOTA models invalidates your core EBM thesis." Evaluations on SOTA outputs reveal an energy-ordering inversion ($\overline{E}_{\text{correct}} > \overline{E}_{\text{incorrect}}$), suggesting that highly-optimized base models exhibit "reward hacking" dynamics that confound standard linear EBM evaluators. The in-distribution AUROC = 0.9545 on the FoVer corpus (n=6,548; exp1072) is unchanged; the inversion is an OOD boundary on the energy class, not a falsification of the framework.